Is the Anion the Major Parameter in the Shape Control of Nanocrystals?†

A. Filankembo,‡ S. Giorgio,§ I. Lisiecki,‡ and M. P. Pileni*,‡

Laboratoire L.M.2.N., U.M.R. C.N.R.S. 7070, Université Pierre et Marie Curie (Paris VI), B.P. 52, 4 Place Jussieu, F-752 31 Paris Cedex 05, France, and CRMC2-CNRS, Campus de Luminy, Case 913, 13288 Marseille Cedex 9, France

Received: October 22, 2002; In Final Form: February 18, 2003

In this paper, copper nanocrystals are produced by using $Cu(AOT)_2$−isooctane−water solution as a template. Even if the template does not change with various salt additions, the nanocrystal growth markedly depends on the salt used. It is demonstrated that chloride ions enable the growth of nanorods with an aspect ratio varying with chloride concentration. Conversely, only a slight amount of bromide ion is needed to increase the nanorod aspect ratio from 3 to 5 without any changes when increasing the bromide ion concentration. A rather large number of cubes are produced. Formations of nanorods and cubes are explained in terms of anion adsorption on (111) and (100) faces, respectively. By replacing chloride by other ions, the morphology of copper nanocrystals drastically changes. In all cases, the nanocrystals formed are fcc single crystals with a polyhedral shape or crystals composed of fcc tetrahedra (deformed or not) bounded by (111) faces. Some cylinders are formed by the connection of 2 different crystals with different 5-fold axes and/or with additional planes. This gives rise to various particle shapes.

I. Introduction

One of the challenges in advanced materials is the control of the inorganic nanocrystal morphology. In fact the shape of nanocrystals influences the physical properties.[1] This is observed for metals, oxides, and semiconductors. Such changes in the physical properties produce a wide range of electrical, optical, and/or magnetic properties and open a new domain of both fundamental and technological interest.

It is well-known that reverse micelles are efficient nanoreactors for producing spherical nanomaterials.[2] However, a careful study of these systems points out a number of discrepancies.[3] (i) The size of the produced material, under the same experimental conditions, is not that of the droplets used as a template. In fact, for II−VI semiconductors (CdS, CdTe, CdMnS) the particle size varies from 2 to 4 nm ,[4] whereas for metals it increases from 2 to 6 nm for silver and 2 to 10 nm for copper[5] and silver sulfide.[6] This control of the particle size is obtained for the smallest water-in-oil droplets (varying from 0.6 to 6 nm), whereas for larger template sizes (from 6 to 12 nm) no changes in the particle size are observed. This was explained in terms of water structure in the droplet.[7] An exception is found for silver sulfide nanocrystals with a linear increase in the particle size with that of the template.[6] It can thus be concluded that the control of the particle size by using reverse micelles not only depends on the template size but also on the material used and the water−oil interface rigidity (bound water). In most cases, spherical nanomaterials are produced. However, various shapes can be made. Hence, reverse micelles of CTAB/butanol/octane are used to produce cubic $KMnF_3$ nanocrystals.[8] Spherical reverse micelles of functionalized surfactant (cadmium diethylhexylsulfosuccinate usually called $Cd(AOT)_2$) with 10 nm average diameter induce the formation of flat equilateral CdS nanocrystals.[9] Similarly, spherical reverse micelles of $Ba(AOT)_2$ or $Ca(AOT)_2$ produce spherical, elongated, and rod-shaped nanocrystals.[1−11] This is observed for $BaCrO_4$ and $CaCO_3$ nanoparticles. This could be due to the presence of impurities and/or additives produced during the chemical reaction in reverse micelles. From this, it is reasonable to conclude that reverse micelles can be used as nanoreactors to produce nanoparticles. In most cases, a spherical template produces nanospheres. However, the hydration of the water pool, procedure mode, production of various species during the chemical reaction, and presence of some impurities and/or additives prevent the control of spherical particles and induce formation of nanoparticles having various shapes.

In 1993 we observed that synthesis of copper nanocrystals in cylindrical reverse micelles permits us to produce a few cylinders and a large amount of spherical nanocrystals.[12] Because of these data and because the same three-component system produces self-assemblies of surfactants having various shapes, we demonstrate that the shapes of colloidal solutions made of functionalized surfactants partially control those of the nanocrystals.[13,14] This control of the nanocrystal shape by that of the template has been recently confirmed by Simmons et al.[15] In fact, it is well-known that addition of phosphatidylcholine to Na(AOT) reverse micelles induces a structural change of the self-assembly with a change of the spontaneous curvature and formation of wormlike, cylindrical, reverse micelles that entangle to form gel-like systems.[16] Syntheses of CdS nanoparticles in such colloidal assemblies make it possible to vary the morphology of the nanocrystals from spheres to nanorods with a switch in the crystal structure from cubic to hexagonal. However, we found out that addition of a very small amount of NaCl (10^{-3} M) to the micellar solution induces formation of nanorods[17] characterized by a high crystallinity of 5-fold symmetry.[18] This was surprising enough to try to understand the influence of salt on nanocrystal growth. By changing the salt in the colloidal solution, we discovered that the copper

† Part of the special issue "Arnim Henglein Festschrift".
* Corresponding author.
‡ Université Pierre et Marie Curie (Paris VI).
§ Campus de Luminy.

10.1021/jp022282q CCC: $25.00
Published on Web 04/10/2003

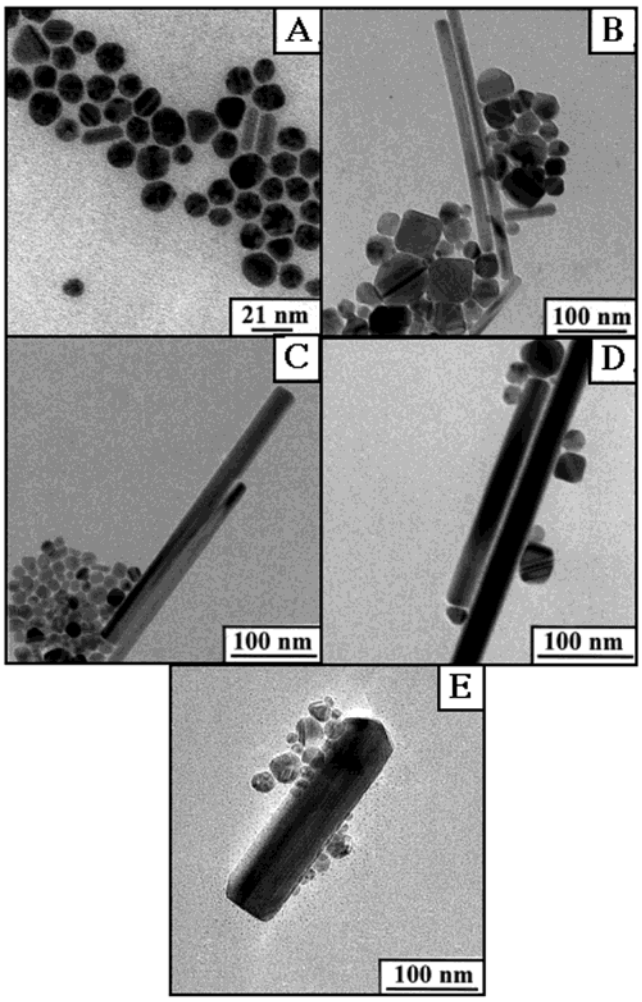

Figure 1. TEM patterns of particles obtained in the presence of sodium chloride (A) [NaCl] = 0; (B) [NaCl] = 5×10^{-4} M; (C) [NaCl] = 1.1×10^{-3} M; (D) [NaCl] = 1.6×10^{-3} M; (E) [NaCl] = 2.2×10^{-3} M.

nanocrystal shape drastically changes with the type of salt added.[19] One of the hypotheses was that the effect could be due to Hofmeister series.[20] It is why a systematic study of salt effects has been developed and is presented in this paper. To try to understand the effect of additives on the nanocrystals growth we have done a careful study of the various papers recently published in this area.[21] Hence, bubbling hydrogen through an aqueous solution containing $PtCl_4^{2-}$ produces cubic platinum nanocrystals.[22,23] Note that no surfactant is needed to obtain cubic nanoparticles. However, the size of the cubes is controlled by polymer addition. Gold nanorods are made by UV−visible irradiation of gold salt solubilized in the bulk phase of normal CTAC micelles.[24] It is difficult to understand the template role of normal micelles. Nanodisks are produced[25] and their sizes[26] depend on the amount of hydrazine present in solution. Again, the key parameter in controlling the nanoparticle shape is not the template but the amount of reducing agent. A convincing experiment showing that the template is not the major parameter in controlling the particle shape is the production of ZnTe[27] and CdTe[28] nanowires by the solvothermal process. In such cases, Zn/Cd metals and their tellurides are heated in the presence of hydrated hydrazine without any surfactant and/or polymer in the solution. From the literature, a general agreement seems to emerge that control of the nanoparticle shape needs to involve a mixture of two surfactants. This has been well demonstrated with various materials such

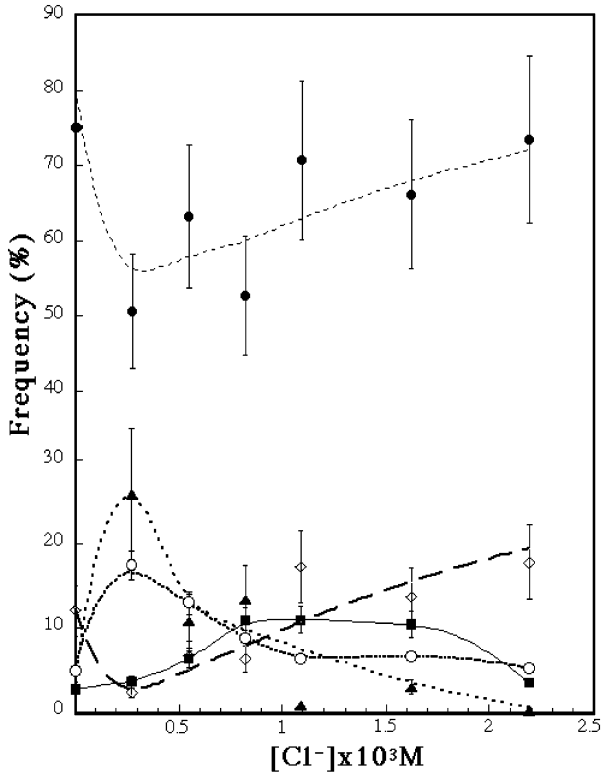

Figure 2. Variation of the relative percentage of nanocrystals differing by their sizes and shapes, spheres (●), triangles (▲), rods and cylinders (O), square (■), and other shapes (◇), with chloride concentration.

as CdSe,[29] cobalt,[30] and iron[31] nanorods. The relative ratio of surfactants controls their aspect ratio. However, such claims are not always valid. In fact, the presence of a single surfactant is enough to control the dimensions of silver and gold nanorods.[32,33] In the latter systems, the ratio of seed to base concentrations is the key parameter in controlling the nanorod aspect ratios. From these data it seems reasonable to conclude that a colloidal solution is a poor template and the control of the particle shape is mainly due to the influence of additives on the nanocrystal growth.

In this paper we demonstrate that salt addition to a colloid template drastically changes the nanocrystal shape.

II. Experimental Section

II.1. Products. Copper(II) bis(2-ethylhexyl)sulfosuccinate $Cu(AOT)_2$ is prepared by ion exchange with the sodium salt as described elsewhere.[34] Residual water present in the initial $Cu(AOT)_2$−isooctane solutions, before addition of water, is analyzed by the Karl Fischer titration method using a Mettler automatic titrator. The $Cu(AOT)_2$ concentration is determined by adding the sample to a solution of 0.03 M hydrochloric acid and 0.3 M ammonium acetate, and subsequently titrating for copper(II) using a 0.01 M sodium EDTA solution with 4-(2-pyridazol)resorcinol as a color indicator.

Isooctane and hexadecyltrimethylammonium bromide, are from Fluka, and ammonium acetate (98%), sodium EDTA, and 4-(2-pyridazol)resorcinol (99%) are from Prolabo. Sodium bromide, potassium bromide, copper chloride dihydrate, sodium fluoride, sodium carbonate, sodium nitrate, and sodium iodide are from Sigma. Sodium perchlorate hydrate, sodium hydrogen phosphate, sodium hydrogen sulfite, and hexadecyltrimethylammonium chloride are from Aldrich, Merck, Riedel de Haen, and Acros Organics, respectively. Salts were dried before use and used without further purification.

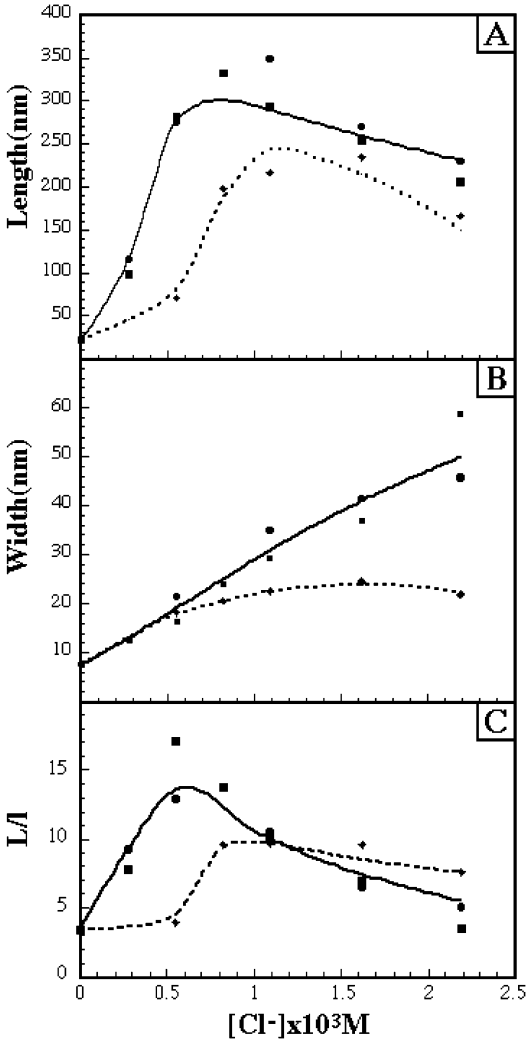

Figure 3. Variation of the length (A), the width (B), and the aspect ratio (C) with chloride concentration. (■) [NaCl], (●) $CuCl_2$, (◆) CTAC. The chemical reaction is ended after 3 h.

II.2. Apparatus. The measurements were made with a Tacussel CD 810 instrument using a TD 100 (platinum) electrode from the same manufacturer.

The transmission electron microscopy (TEM) experiments were carried out using a Philips EM300 at 300 kV, a JEOL 200CX at 200 kV, and a JEOL 4000 EX at 400 kV.

III. Hofmeister Series

The Hofmeister series[20] was discovered a century ago. It is based on the change in the solubility of organic molecules dissolved in aqueous solution. The solubility of various molecules such as alcohol, polymer, surfactant, protein, etc..., is adjusted by salt addition.[35−37] The anions and cations can be classified in the so-called Hofmeister series:

$$SO_4^{2-} > CO_3^{2-} > HPO_4^{2-} > F^- > Cl^- > Br^- > NO_3^- > I^- > ClO_4^- > SCN^-$$

$$Na^+ > K^+ > Li^+ > Rb^+ > Cs^+$$

This series is universal in that the order of the sequence does not depend on the nature of the organic molecules. It is observed for very high salt concentration. This solubility effect is more pronounced for anions than cations. A low solubility of organic molecules (salt out) is obtained by using salts on the left side of the series. On changing the salt from left to right, the solubility increases to reach a zone in which it is higher than that obtained in pure aqueous solution (salting in). This Hofmeister series is observed in various domains such as biology and/or colloidal solution. In fact, the efficiency of a chemical reaction catalyzed by an enzyme markedly change with salt addition. Similarly in colloidal solution, addition of a salt induces changes in the water structure. For a salt on the left-hand side, the anions desorb at the water−oil interface and then decrease the solubility between water and surfactant. The water is more structured and is like ice. This was confirmed by surface-specific vibration spectroscopy[38] and means the water molecules are highly bound to the surfactant. From left to right the water structure evolves to that of the bulk phase and then to a more destructured water solution.

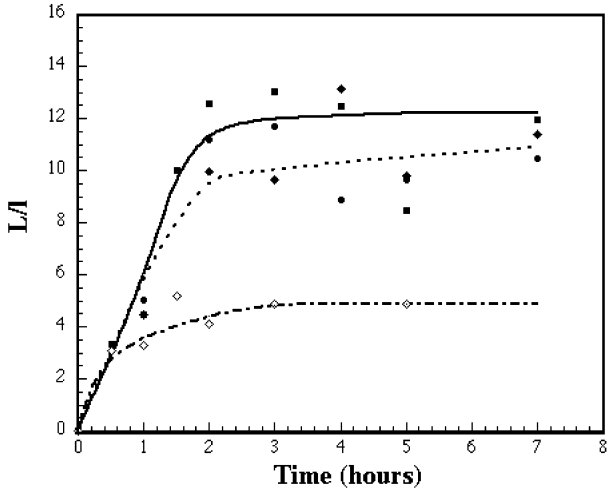

Figure 4. Variation of the length-to-width ratio of nanorods at $[Cl^-] = 0.84 \times 10^{-3}$ M with time. (■) [NaCl], (●) $CuCl_2$, (◆) CTAC. The chemical reaction is ended after 3 h.

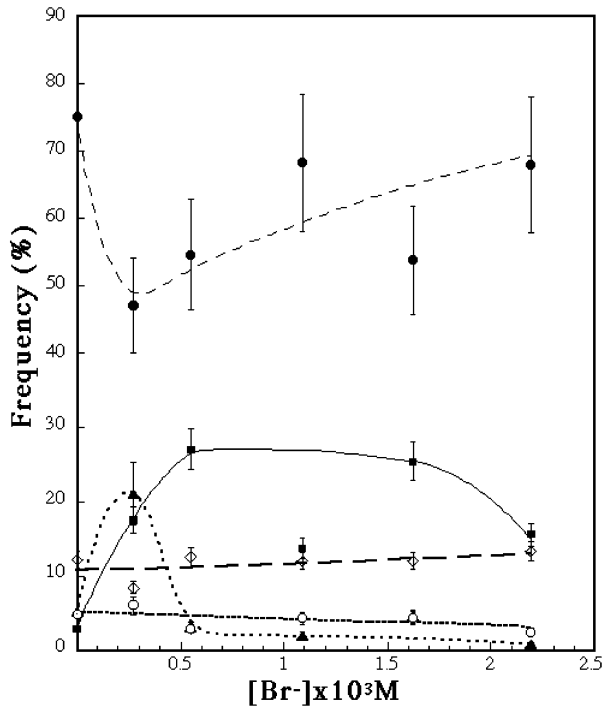

Figure 5. Variation of the relative percentage of nanocrystals differing by their sizes and shapes [spheres (●), triangles (▲), rods and cylinders (O), square (■), and other shapes (◇)] with bromide concentration.

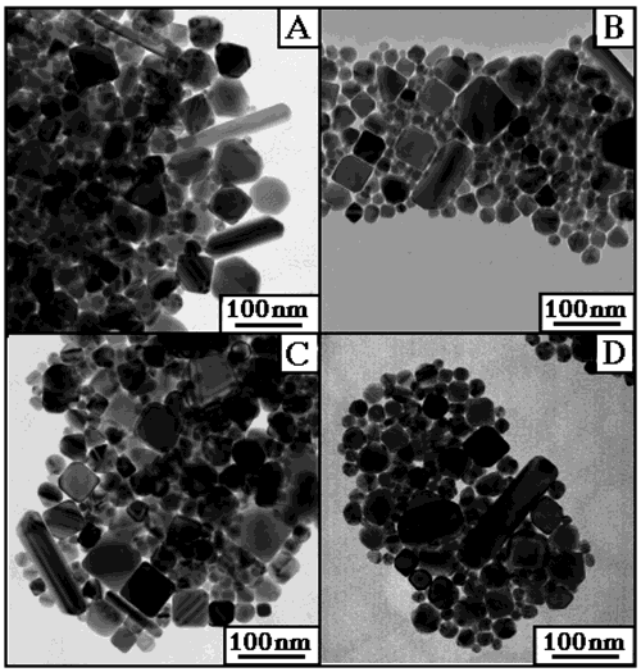

Figure 6. TEM patterns of nanocrystals obtained in the presence of sodium bromide. The chemical reaction is ended after 3 h. (A) [NaBr] = 2.5×10^{-4} M; (B) [NaBr] = 1.1×10^{-3} M; (C) [NaBr] = 1.6×10^{-3} M; (D) [NaBr] = 2.2×10^{-3} M.

IV. Synthesis of Copper Nanorods

The surfactant used to make the template is highly purified (≤1% of salt impurities), copper(II) bis(2-ethylhexyl)sulfosuccinate, usually called $Cu(AOT)_2$. The water content is defined as the ratio of the water to surfactant concentration, $w = [H_2O]/[AOT]$. $Cu(AOT)_2$ (5×10^{-2} M) is solubilized in isooctane and water is added to the solution with $w = 10$. The sample is vigorously shaken and centrifuged for 15 min at 4500t.mn. The system is well characterized.[19] At this water content, it consists of three phases with very flat menisci, of ultralow interfacial tension which separate all the phases.[39] The upper phase is isooctane without any detectable $Cu(AOT)_2$ molecules. The middle phase is birefringent with coexisting planar and onion phases. The volume of the birefringent phase is too small to allow any structural studies. The lower phase is optically clear and made of interconnected cylinders. After 22 h, hydrazine solubilized in water is added to the solution. Hydrazine is added so that the overall water content and hydrazine concentration are fixed at 10 and 0.15 M, respectively. Either at the end of the synthesis (3 h) or at a given time, *t*, a drop of solution is deposited on a TEM grid.

On replacing water with an aqueous solution containing various salts having a rather low overall concentration ([salt] ≤ 2.5×10^{-3} M), the phase diagram of $Cu(AOT)_2-H_2O-$isooctane does not drastically change. The three phases remain present and only slight changes in the relative volumes of birefringent and isotropic phases are observed (Table 1). The birefringent phase is still a mixture of an onion and a planar phase; while the former does not change, the latter becomes wavelike. The conductivity of the isotropic phase remains very high and does not change with salt addition (Table 1). The data deduced from SAXS measurements of the isotropic phase do not change. The slight variations given in Table 1 are close to the experimental errors (10%). Note that the slight structural change on salt addition does not depend on the type of salt added.

TABLE 1: Relative Volume of the Isotropic Phase (V_{is}), the Birefrigent (V_b), and Isooctane (V_i), the Characteristic Diameter of Cylinders (*d*), the Head Polar Group Area (*s*), and the Conductivity of the Isotropic Phase ([$Cu(AOT)_2$] = 5×10^{-3} M, $w = 10$)

salt	V_i	V_{is}	V_b	*d* (Å)	s (Å^2)	κ (S/m)
none	0.83	0.14	0.03	30	40	1.2
NaCl	0.84	0.14	0.02	32	38	1.3
KCl	0.84	0.15	0.01	32	38	1.2
$Cu(Cl)_2$	0.84	0.15	0.01	32	38	1.2
CTAC	0.84	0.15	0.01	32	38	1.4
NaBr	0.84	0.16	0.01	32	38	1.3
KBr	0.83	0.16	0.01	32	38	1.3
$NaNO_3$	0.84	0.16	0.01	32	38	0.7
Na_2SO_4	0.80	0.16	0.04	32	38	1.3
NaF	0.78	0.16	0.06	32	38	1.2
$NaHSO_3$	0.82	0.17	0.01	32	38	1.6

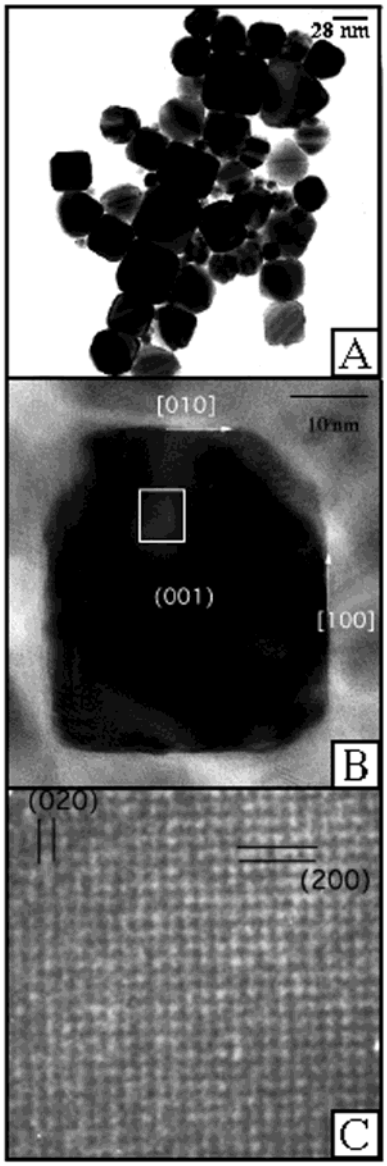

Figure 7. (A) Organization of square copper nanocrystals in 2D superlattices. (B) TEM image of an isolated nanocrystals. (C) HRTEM image of the cube observed in B.

V. Results

Copper nanocrystals produced in the absence of salt differ by their sizes and shapes (Figure 1A). The relative percentages of various shapes (Figure 2) are estimated from a population higher than 500 particles. Triangles (3%), spheres (80%), squares

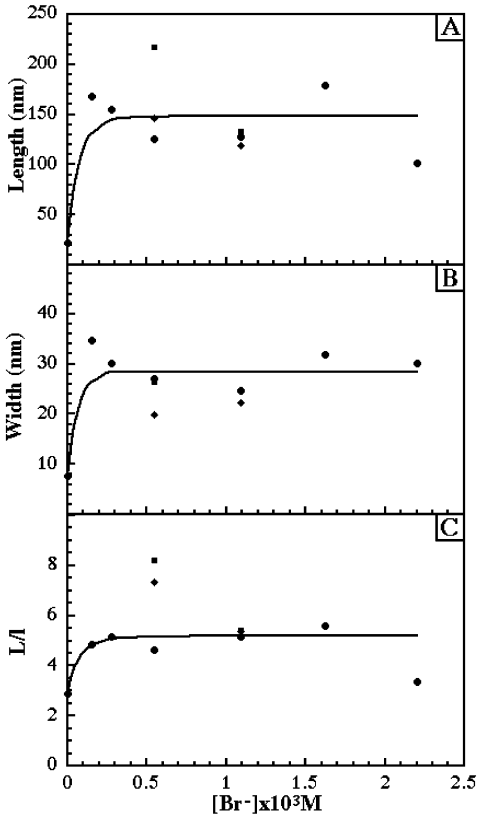

Figure 8. Variation of the length (A), the width (B), and the aspect ratio (C) with bromide concentration. The chemical reaction is ended after 3 h.

(2%), cylinders (4%), and other types of shapes such as decahedron, etc....(11%) are formed. All these nanocrystals are highly crystallized without traces of copper oxide. This is observed under various experimental conditions and shown below.

Addition of NaCl induces changes in the relative percentages of nanocrystals differing by their shapes (Figure 2) which vary with chloride concentration. The percentage of spherical nanocrystals is rather large (between 60 and 80%). It decreases and then increases. The percentage of triangles and nanorods increases to reach a maximum at [NaCl] $= 2 \times 10^{-4}$ M and then decreases. The percentage of cubic particles increases to reach a maximum around 10% and then decreases, whereas those of other shapes increase slightly. Let us first consider nanorods produced at various NaCl concentrations. Figure 1 shows large nanorods obtained by increasing the NaCl concentration (from A to E). The number of rods is negligible compared to other nanocrystals (Figure 2). However, because the nanorods are very large, the number of copper atoms involved in their fabrication is significant. The length of the nanorods increases with increasing NaCl concentration to reach a maximum at around 8×10^{-4} M, whereas the width increases continuously (Figure 3). The aspect ratio of the nanorods increases with increasing NaCl concentration to reach a maximum at 6×10^{-4} M. Their kinetic growth shows an increase in the aspect ratio with time to reach a plateau 2 h after the chemical reaction starts (Figure 4). From these data, it is concluded that addition of NaCl induces drastic changes in the nanocrystal shapes with appearance of nanorods having an aspect ratio depending on the NaCl concentration added to the colloidal solution before the synthesis. This confirms previous data.[40] By replacing NaCl by KCl, data similar to those obtained with NaCl are obtained (same change in length, width, and aspect ratio with Cl^- concentration). This indicates no effect of the salt cation on the nanocrystal growth. Such results indicate that chloride ions seem to be the major factor in the control of the nanorod aspect ratio. To confirm this, two other chloride derivatives are used. The first is a divalent salt, copper chloride, $CuCl_2$, which demonstrates the effect of chloride ions and that of the ionic strength. The second is cetyltrimethylammonium chloride, CTAC, to check the interfacial influence.

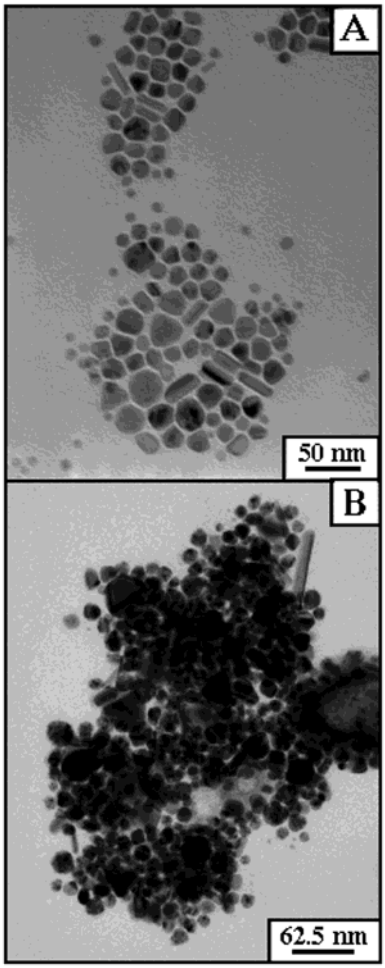

Figure 9. TEM image in the presence of 10^{-3} M of NaF (A) and NaI (B).

(i) In presence of $CuCl_2$, the same behavior as that with NaCl is observed. The increases in length and width with increasing the chloride ion concentration remain the same (Figure 3). The variation of the nanorod aspect ratio with chloride concentration is confirmed with a maximum around 12 as observed with NaCl. The kinetic growth of nanorods is the same as that obtained with NaCl (Figure 4). These data clearly show that formation of nanorods is due to the presence of chloride ions during the crystal growth and does not depend on the ionic strength which increases from C to $^3/_2C$ (where C is the salt concentration) by replacing NaCl by $CuCl_2$. Hence, chloride ion is the key factor in controlling the nanorod growth. The colloidal template makes possible the seed formation, and the selective adsorption of chloride ions favors forming nanorods. This will be discussed below.

(ii) With CTAC,the general behavior is similar to that observed with NaCl and $CuCl_2$ (Figure 3), indicating that chloride ions are the key parameter in nanorod growth. However some slight discrepancies are observed: Figure 3 shows an increase in the length with CTAC concentration and the

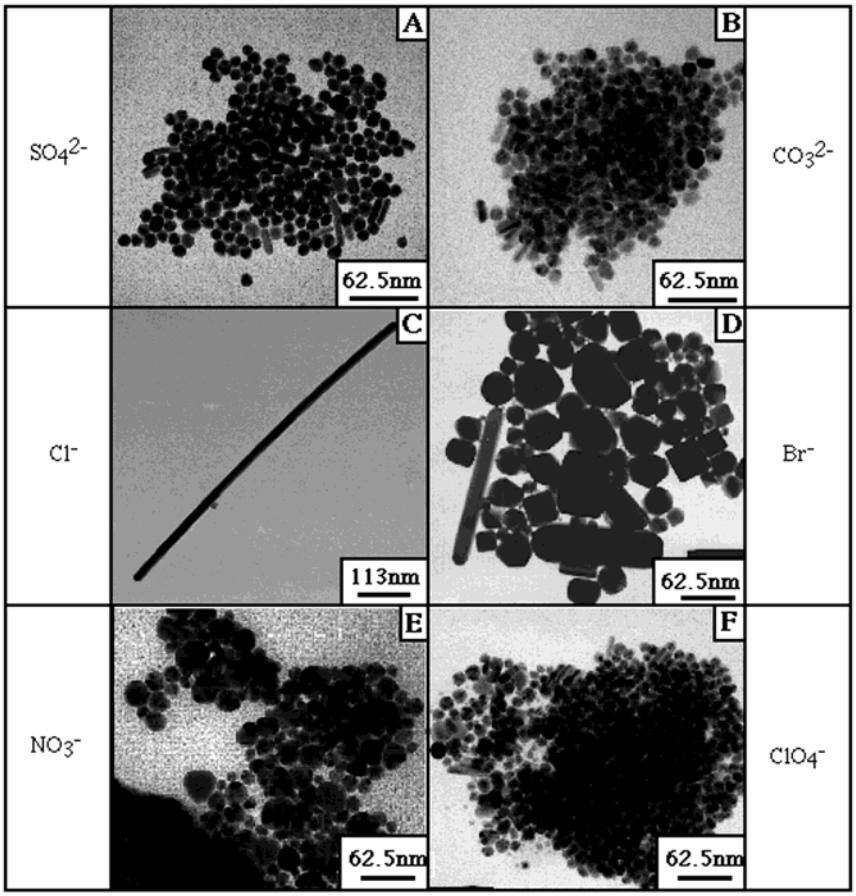

Figure 10. TEM images of nanocrystals obtained by adding 10^{-3} M of various salts. The chemical reaction is ended after 3 h. (A) Na_2SO_4, (B) Na_2CO_3, (C) NaCl, (D) NaBr, (E) $NaNO_3$, and (F) $NaClO_4$.

maximum is reached at [CTAC] = 1.1×10^{-3} M instead of 7×10^{-4} M. The width increases very slowly compared to that obtained with NaCl and $CuCl_2$. The aspect ratio reaches a maximum at [CTAC] = 8×10^{-4} M instead of 6×10^{-4} M and it is less (10) than those obtained with NaCl and $CuCl_2$ (12). Hence the variation in length, width, and aspect ratio of nanorods at various CTAC concentrations are not homothetic compared to those obtained for NaCl, KCl, and $CuCl_2$. This indicates that Na^+, Cu^{2+}, and K^+ do not selectively adsorb on various faces whereas this is observed for several ammonium derivatives.[41,42] From this, it is expected that CTA^+ plays a role in nanocrystal growth. Note that the kinetic growth of nanorods is the same as that observed for the other chloride ions (Figure 4) with a smaller aspect ratio.

By replacing NaCl by NaBr, as is clearly shown in Figure 5, there are changes in the percentages of the various shapes produced. The relative amounts of spheres and triangles remains similar to those produced in the presence of chloride ions (Figure 2). Figure 6 shows that, conversely to Cl^-, on Br^- addition, the relative amount of nanorods decreases but then retains the same percentage with increasing Br^- concentration. A drastic increase in cubic nanocrystal percentage is observed and reaches almost 27% of the produced nanocrystals. By replacing NaBr by CTAB, the number of cubes produced is much larger than that obtained with NaBr and with a size distribution of cubes low enough to enable organization of squares on a substrate (Figure 7A). The structural study of these cubes shows formation of rather large particles (40 nm) limited at the top by [001] faces, and truncated at the corners (Figure 7B). The HRTEM image of the lattice shows that the nanocrystals are fcc [001] oriented without structural defects (Figure 7C).

Let us consider nanorods. Figure 6 shows a marked change in the behavior by replacing Cl^- by Br^-. Figure 8 shows that at low bromide concentration, [Br^-] < 1.5×10^{-4} M, their length and width markedly increase with Br^- concentration. The aspect ratio increases from 3 to 5. Above [Br^-] = 1.5×10^{-4} M, no changes in length, width, and aspect ratio are observed. Such behavior markedly differs from that observed with Cl^- and shown in Figure 3. Surprisingly, the kinetic of growth remains the same as that obtained with Cl^- (Figure 4). The formation of nanorods and cubes could be due to the presence of halide anion in the colloidal template. Experiments similar to those described above are performed by replacing NaCl by either NaF or NaI. (i) On 10^{-3} M NaF addition to the template ($Cu(AOT)_2$−water−isooctane), there are no changes in shapes and sizes (Figure 9A) compared to what is observed in absence of salt (Figure 1A). This indicates that the slight change in the structural template due to salt addition does not play a role in the change of the nanocrystal shape observed above with Cl^- and Br^-. (ii) With 10^{-3} M NaI, a large variety of shapes with a large size distribution is observed (Figure 9B). From data obtained with NaF and NaI it is concluded that the halide series is not involved in the control of nanocrystal growth. Similar selective adsorptions by chloride and bromide ions on a Pt surface used as an electrode were observed.[43] This was explained in terms of hydration, size, and electronegativity of the anions. These physical processes cannot be involved in our experiments because the same data are obtained with F^- and I^-, which correspond to the two extremes in the progression of these various factors.

We know from the literature that the presence of a large amount of salt changes the solubility of organic molecules.[20,35,36]

This has been generalized for various systems. To confirm the fact that the Hofmeister series does not play a role in the nanorod growth, syntheses are performed with the various salts of this series. The salt concentration remains unchanged (10^{-3} M) and the nanocrystals are deposited after 3 h on a carbon grid. Figure 10 shows TEM images of nanocrystals obtained in the presence of various salts under the same experimental conditions ([anion] = 10^{-3} M). The top left of the figure is the TEM image obtained when the synthesis is performed in the presence of SO_4^{2-} (Figure 10A) corresponding to the left of the Hofmeister series. The last one (Figure 10F) is obtained with ClO_4^- corresponding to the right of the series. Similar patterns are obtained with other salts (Figure 10). Obviously from this, except with Cl^- and Br^-, no drastic change in the shape of nanocrystals is observed. This clearly indicates that the control of nanorods and cubic copper nanocrystals is not related to the Hofmeister series as could be expected. This also excludes the influence of the anion polarizability.[43] In fact, the polarizability of these anions decreases as follow: $F^- < Cl^- < NO_3^- < Br^- < ClO_4^- < SO_4^{2-} < I^-$. With F^-, SO_4^{2-}, NO_3^-, I^-, and ClO_4^{2-}, the patterns obtained in the presence of 10^{-3} M of anions are similar to those in their absence. This indicates that neither F^- (Figure 9A), SO_4^{2-} (Figure 10A), NO_3^- (Figure 10E), I^- (Figure 9B), nor ClO_4^- (Figure 10F) selectively adsorb on a given face. This confirms that the Hofmeister series does not play any role in nanorod growth.

As already stated, whatever the salt is, quite a large number of nanocrystals differ by their shapes. As examples, high-resolution transmission electron microscopy, HRTEM, measurements are made of nanocrystals differing by their shapes. Figures 11 and 12 list some of these nanocrystals: large, (110)-oriented, polyhedral copper nanocrystals are formed (Figure 11A). The black arrows give the directions limiting the nanocrystal. The magnification shown in Figure 11B corresponds to the fcc structure without defects with the (002) and (111) lattice fringes. A view from above of the 3D shape is shown in Figure 11C. The particle is mostly limited by (111) faces and truncated by (100) faces. The anisotropy ratio of the surface free energies corresponding to the equilibrium form of a polyhedron with that shape is $\sigma_{100}/\sigma_{111} = 1.02$. It corresponds to the case of large gold particles (a few micrometers), at a temperature close to the melting point.[44] Large flat nanocrystals (6 nm) [111]-oriented and limited by (111) faces at the top, the bottom and the edges are produced (Figure 11D). They are truncated at the 3 corners by less extended (100) faces. The arrows indicate the main directions. The HRTEM image (Figure 11E) shows a perfect fcc lattice without defects. The 3 sets of fringes correspond to the reflections (1/3 (−422)) which are observed in atomically flat, noble metal samples.[45] The 3D shape is drawn in top view and in cross section in Figure 11F. The anisotropy ratio of the surface free energies corresponding to a polyhedron with that shape is $\sigma_{100}/\sigma_{111} = 1.4$, which is larger than the values usually observed in fcc nanocrystals at equilibrium.[44] Other more complicated structures are found among the nanocrystals. Figure 12A shows a particle composed of 5 deformed fcc tetrahedrals bounded by (111) planes,[46] with two more developed sectors (at the left side). According to the magnification of the center in Figure 12B, the upper sector on the right side contains 2 sets of (111) lattice planes, so that it is not too far away from the (110) orientation. The 5-fold axis is tilted compared to the direction of observation. Figure 12C shows a large cylinder (52-nm long) formed by the connection of 2 different crystals with different 5-fold axes. Each crystal is a large truncated decahedron made of 5 fcc deformed tetrahedra bounded by (111) planes

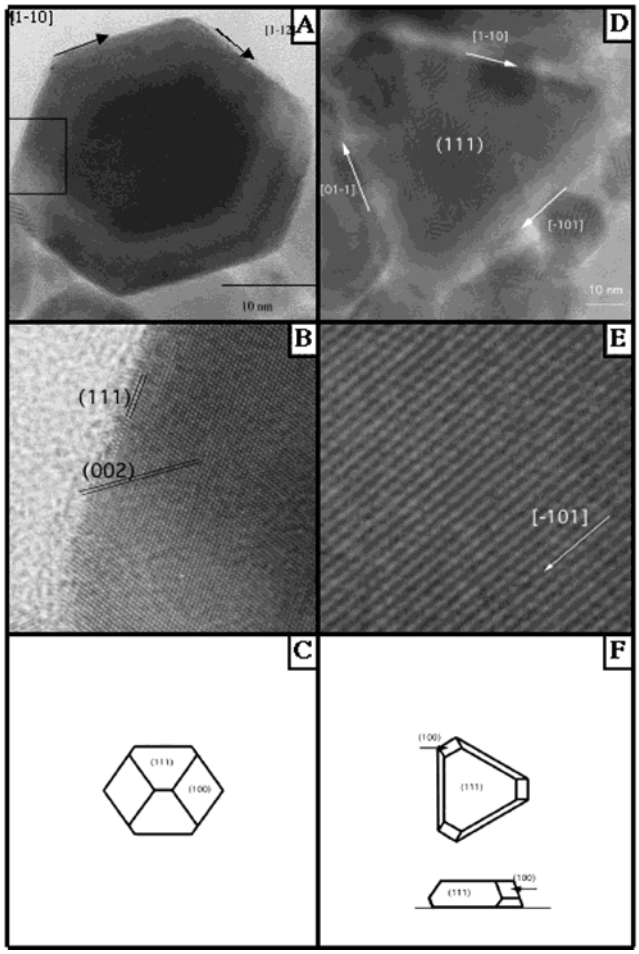

Figure 11. TEM patterns of nanocrystals differing by their shapes. A and D at low magnification, B and E are high-resolution TEM images of shapes shown on A and D. C and F are 3D shapes observed in A and D.

as described previously and elongated along some sectors. An enlarged HRTEM image corresponding to the 5-fold symmetry centers is shown in Figure 12D. The sector at the right side is oriented normal to a [110] direction. Similarly, a cylindrical particle is seen in Figure 12 E, composed of a set of deformed fcc tetrahedra bounded by (111) faces parallel to the 5-fold axis with additional planes. Figure 12F shows an enlarged HRTEM image with the lattice seen along a [110] direction. This means that the lateral face limiting the cylinder at the right side is a (001) face, which is consistent with the model described in previous work. All these structures differ. However, all the cylinders are made of deformed fcc tetrahedra bounded by (111) faces, limited by 5 (111) faces at each extremity of the cylinder, and limited on the lateral edges by (001) faces. Also, some cylinders are twinned.

VI. Discusssion

These nanocrystals are synthesized in a template made of surfactant [$Cu(AOT)_2$] = 5×10^{-2} M), isooctane, and water ([H_2O] = 5×10^{-1} M). The template structure slightly changes on salt addition ([salt] = 10^{-3} M). Table 1 shows that the structural change does not depend on the salt used. Hence, whatever the salt is, the template remains the same. Figure 10 clearly shows that the nanocrystal shapes depend on the salt used. This indicates that the structure of the template is not the major parameter in the control of nanomaterial shape. This is confirmed by the fact that in the presence of various salts

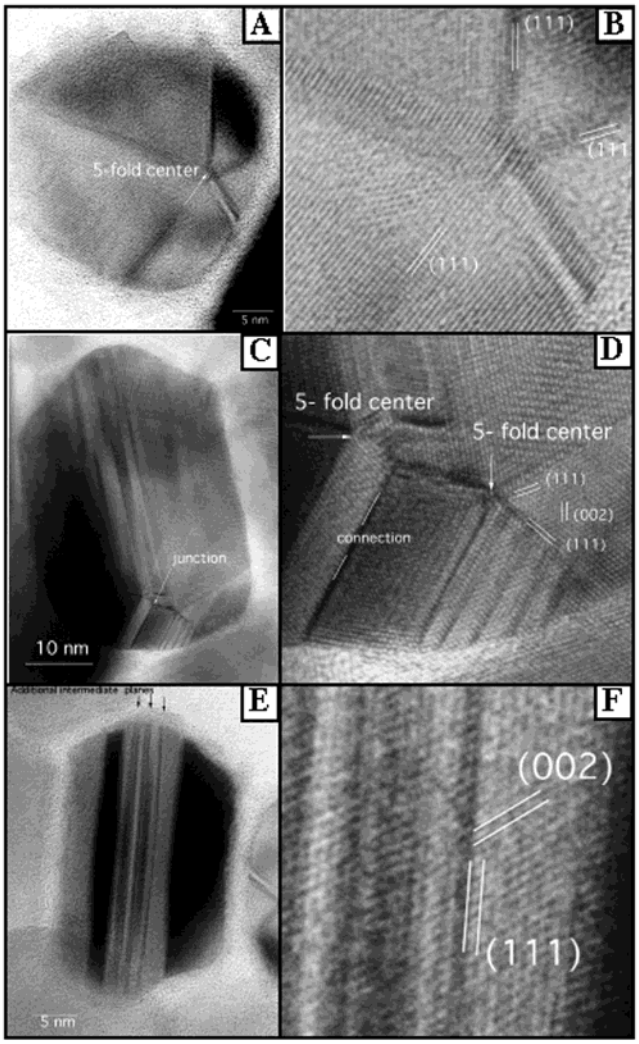

Figure 12. TEM patterns of nanocrystals differing by their shapes. A, C, and E at low magnification. Same structures B, D, and F, respectively, at high magnification.

(Figures 9 and 10) and in absence of additives, the shapes of various copper nanocrystals produced do not change. Figure 10 shows that the major change in the nanocrystal shapes is observed by addition of chloride and bromide ion. In particular, nanorods and cubes are produced. The nanorod structure was investigated in previous work and is characterized by a truncated decahedral 5-fold symmetry.[18] This clearly indicates that the particle growth is hindered and takes place in the [110] direction, i.e., the 5-fold axis resulting in well-defined long rods. The cylinders are limited at the edges by (001) faces and at each extremity by 5 (111) faces. The formations of cylinders and/or nanorods and that of cubes are determined from the preferential growth of the (001) faces compared to the growth of (111) faces.

With chloride ions, produced by addition of NaCl, KCl, or $CuCl_2$ in the template, the length of nanorods with increasing the salt concentration reaches a maximum at $[Cl^-] = 8 \times 10^{-4}$ M whereas the width continuously increases with chloride concentration. These processes are attributed to selective adsorption of chloride ions on (001) and (111) faces. At low Cl^- concentration, the anions adsorb preferentially on (001) faces and the growth is faster on the (111) faces. Conversely, at high Cl^- concentration, Cl^- also adsorbs on (111) faces. Hence, Cl^- preferentially adsorbs on (001) faces. When the amount of Cl^- is large enough, adsorption on (111) faces takes place.

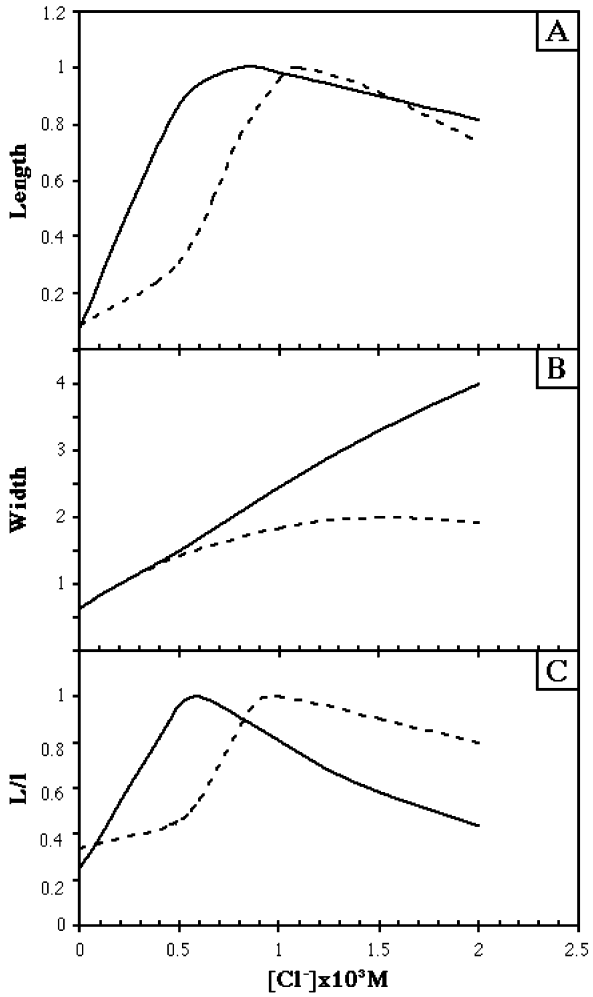

Figure 13. Normalization to unity of Figure 3.

By replacing NaCl, KCl, and $CuCl_2$ by CTAC, similar behavior is observed with an increase in the nanocrystal length to a maximum whereas the width continuously increases with increasing CTAC concentration. However, the variation of length and width of nanocrystals with increasing chloride ion concentration is not exactly the same (Figure 3). To point out these changes between NaCl, $CuCl_2$, and CTAC, the curves in Figure 3 are normalized (Figure 13). The maximum length, the width obtained for a chloride concentration of 2×10^{-4} M, and the maximum aspect ratio are normalized to 1. Figure 13A shows, at low Cl^- concentration, more or less the same increase in the length with NaCl, $CuCl_2$, and CTAC. However, this increase takes place at higher CTAC concentration than those of the others. This is attributed to the fact that the number of "free" chloride ions is less with CTAC than NaCl (or $CuCl_2$). This is due to the strong interactions between the head polar group of the surfactant and its counterion. This has been well demonstrated with various surfactants. Figure 13A shows, at high chloride concentration, that there is a faster decay of the length in the presence of CTAC than that obtained with NaCl or $CuCl_2$. This indicates that CTA^+, like other ammonium derivatives,[41,42] adsorbs on (111) faces, preventing the crystal growth. Similarly the increase in the width with chloride ions is slower compared to that observed with other salts (Figure 13B). This indicates that CTA^+ adsorbs on (001) faces as well as on (111) faces. However, the influence of CTA^+ seems to be more efficient on the width than on the length of nanorods, indicating a stronger adsorption of (001) faces compared to (111). This behavior is confirmed from the decay of the aspect

ratio, where its decay at high Cl^- concentration is slower in the presence of CTAC (Figure 13C) than with NaCl (or $CuCl_2$).

With bromide ions, nanorods and cubes are formed. Conversely to what is observed with chloride ions, only a very low concentration of bromide ($[(Br^-] < 1.5 \times 10^{-4}$ M) is needed to control the aspect ratio of nanorods (Figure 8). No change in the aspect ratio is obtained by increasing the Br^- concentration. Hence a drastic change in the behavior is observed with chloride and bromide ions indicating a strong adsorption of Br^- on various faces. At low Br^- concentration, the growth is faster on the (111) faces than on the (001). However Br^- is more strongly adsorbed on the (111) faces than Cl^-, limiting the aspect ratio of nanorods. In the presence of CTAB a larger number of cubes are produced, indicating that both Br^- and CTA^+ adsorb. Formation of well-defined cubes indicates selective adsorption on (111) and (001). This is mainly due to bromide ions, but also to cetyltrimethylammonium ions.

Similar selective adsorptions by chloride and bromide ions on a Pt surface used as an electrode were observed.[47]

VII. Conclusions

In this paper it is demonstrated that the colloidal template plays a role in the nanocrystal growth with formation of nanoparticles characterized by a very high crystallinity. However, the major role seems to be that of the salt additives. Hence, the control of the particle shape is mainly obtained by addition of chloride and bromide ions inside the template, before the chemical reaction takes place. It is demonstrated that both chloride and bromide ions selectively adsorb on the (001) and (111) faces to favor either crystal growth on the [110] direction or to form cubes. The presence of the ammonium group also perturbs the nanocrystal growth by specific adsorption. Conversely to what could be expected, Hofmeister series does not control the particle shape. From these data it is concluded that salts and/or impurities inside the colloidal template play the major role in the anisotropic nanocrystal growth.

Acknowledgment. The authors thank Dr. Ph. Dubuisson and his group of DTA/DECM/SRMA, CEA−Saclay, Drs. P. Beaunier and F. Warmont of UPMC, Service de Microscopie Electronique à Transmission, Dr. A. Loiseau of ONERA Chatillon, and Dr. J. M. Penisson of the CEA−Grenoble for providing us with facilities for using the transmission electron microscopes.

References and Notes

(1) *Nanostructured Materials*; Shalaev, V. M., Moskovits, M., Eds.; ACS Symposium Series 679; American Chemical Society: Washington, DC, 1997.
(2) Pileni, M. P. *J. Phys. Chem.* **1993**, *97*, 6961.
(3) Pileni, M. P. *Langmuir* **1997**, *13*, 3266.
(4) Pileni, M. P. *Catal. Today* **2000**, *58*, 151.
(5) Lisiecki, I.; Pileni, M. P. *J. Phys. Chem.* **1995**, *99*, 5077.
(6) Motte, L.; Billoudet, F.; Pileni, M. P. *J. Phys. Chem.* **1995**, *99*, 16425.
(7) Motte, L.; Lisiecki, I.; Pileni, M. P. *Hydrogen Bond Networks NATO*. Eds. Dore, J., Bellisan, M. C., Publisher, **1994**; p 447.
(8) Agnoli, F.; Zhou, W. L.; O'Connor, C. J. *Adv. Mater.* **2001**, *13*, 1697.
(9) Pinna, N.; Weiss, K.; Urban, J.; Pileni, M. P. *Adv, Mater*. **2001**, *13*, 261.
(10) Li, M.; Schnablegger, H.; Mann, S. *Nature* **1999**, *402*, 393.
(11) Hopwood, J. D.; Mann, S. *Chem. Mater.* **1997**, *9*, 1819.
(12) Lisiecki, M. P.; Pileni, M. P. *J. Am. Chem. Soc.* **1993**, *115*, 3887.
(13) Tanori, J.; Gulik-Krzywicki, T.; Pileni, M. P. *Langmuir* **1997**, *13*, 632.
(14) Tanori, J.; Pileni, M. P. *Langmuir* **1997**, *13*, 639.
(15) Simmons, B. A., et al. *Nanoletters* **2002**, *2*, 263.
(16) Scartazzini, R.; Luisi, P. *J. Phys. Chem.* **1988**, *92*, 829.
(17) Tanori, J.; Pileni, M. P. *Adv. Mater.* **1995**, *7*, 862.
(18) Lisiecki, I.; Filankembo, A.; Sack-Kongehl, H.; Weiss, K.; Pileni, M. P.; Urban, J. *Phys. Rev B* **2000**, *61*, 4968.
(19) Lisiecki, I.; André, P.; Filankembo, A.; Petit, C.; Tanori, J.; Gulik-Krzywicki, T.; Ninham, B. W.; Pileni, M. P. *J. Phys. Chem.* **1999**, *103*, 9168 and 9176.
(20) Hofmeister, F. *Arch. Exp. Pathol. Pharmakol.* **1888**, *24*, 247.
(21) Pileni, M. P. *Nature Mater.* **2003**, *2*, 145.
(22) Ahmadi, T. S.; Wang, Z. L.; Green, T. C.; Heinglein, A.; El Sayed, M. A. *Science* **1996**, *272*, 1924.
(23) Ahmadi, T. S.; Wang, Z. L.; Heinglein, A.; El Sayed, M. A. *Chem. Mater.* **1996**, *8*, 1161.
(24) Esumi, K.; Matsuhira, K.; Torigoe, K. *Langmuir* **1995**, *11*, 3285.
(25) Maillard, M.; Giorgio, S.; Pileni, M. P. *Adv. Mater.*, in press.
(26) Maillard, M.; Giorgio, S.; Pileni, M. P. Submitted.
(27) Li, Y.; Ding, Y.; Wang, Z. *Adv. Mater.* **1999**, *11*, 847.
(28) Li, Y.; Liao, H.; Ding, Y.; Fan, Y.; Zhand, Y.; Quian, Y. *Inorg. Chem.* **1999**, *38*, 1382.
(29) Manna, L.; Scher, E. C.; Alivisatos, A. P. *J. Am. Chem. Soc.* **2000**, *122*, 12700.
(30) Puntes, V. F.; Kristhnan, K. M.; Alivisatos, A. P. *Science* **2001**, *291*, 2115.
(31) Park, S. J.; Kim, S.; Lee, S.; Khim, Z. G.; Char, K.; Hyeon, T. *J. Am. Chem. Soc.* **2000**, *122*, 8581.
(32) Jana, N. R.; Gearheart, L.; Murphy, C. J. *Chem. Commun.* **2001**, 617.
(33) Jana, N. R.; Gearheart, L.; Murphy, C. J. *J. Phys. Chem. B* **2001**, *105*, 4065.
(34) Petit, C.; Lixon, P.; Pileni, M. P. *Langmuir* **1991**, *7*, 2620.
(35) Collins, K. D.; Washabaugh, M. *Q. Rev. Biophys.* **1985**, *18*, 323.
(36) Franks, K.; In *Water—A. Comprehensive Treatise*; Franks, , Ed.; Plenum: New York, 1973; Vol. 2, p 1.
(37) Eagland, D.; In *Water—A. Comprehensive Treatise*; Franks, , Ed.; Plenum: New York, 1973; Vol. 4, p 305.
(38) Baldelli, S.; Schnitzer, C.; Campbell, D. J.; Shultz M. J. *J. Phys. Chem.* **1999**, *103*, 2789.
(39) Filankembo, A.; Pileni, M. P. *J. Phys. Chem.* **2000**, *104*, 5867.
(40) Pileni, M. P.; Ninham, B. W.; Gulik-Krzywicki, T.; Tanori, J.; Lisiecki, I.; Filankembo, A. *Adv. Mater.* **1999**, *11*, 1358.
(41) Koryta, J. *Electrochim. Acta* **1962**, *6*, 67.
(42) Gierst, L.; Tondeur, J.; Nicolas, E. *J. Electroanal. Chem.* **1965**, *10*, 397.
(43) Leotidis, E. *Curr. Opin. Colloid Interface Sci.* **2002,** *7*, 81.
(44) Heyraud, J. C.; Métois, J. J. *Acta Metall.* **1980**, *28*, 1789.
(45) Kirkland, E. J. *Proc. R. Soc.* **2000**, *122*, 4631.
(46) Graoui, H.; Giorgio, S.; Henry, C. R. *Philos. Mag. B* **2001**, *81* (11), 1649.
(47) Zolfaghari, A.; Conway, B. E.; Jerkiewicz, G. *Electrochim. Acta* **2002**, *47*, 1173.